AN ELECTRONIC JOURNAL OF THE
SOCIETAT CATALANA DE MATEMÀTIQUES

A Hybridizable Discontinuous Galerkin phase-field model for brittle fracture

*Alba Muixí
Universitat Politècnica de Catalunya
alba.muixi@upc.edu

Sonia Fernández-Méndez
Universitat Politècnica de Catalunya
sonia.fernandez@upc.edu

Antonio Rodríguez-Ferran
Universitat Politècnica de Catalunya
antonio.rodriguez-ferran@upc.edu

∗Corresponding author

Resum *(CAT)*

Els models *phase-field* per a fractura fràgil descriuen les fractures com a zones danyades mitjançant un camp continu que varia abruptament entre els estats intacte i trencat. Computacionalment, les malles han de ser fines a prop de la fractura per capturar bé la solució. Presentem una formulació HDG per a un model *phase-field* quasi-estàtic, basada en un esquema alternat a l'hora de resoldre el sistema. La motivació per a utilitzar HDG és que permet la implementació d'estratègies d'adaptabilitat espacial de manera senzilla.

Abstract *(ENG)*

Phase-field models for brittle fracture consider smeared representations of cracks, which are described by a continuous field that varies abruptly in the transition zone between unbroken and broken states. Computationally, meshes have to be fine locally near the crack to capture the solution. We present an HDG formulation for a quasi-static phase-field model, based on a staggered approach to solve the system. The use of HDG for this model is motivated by the suitability of the method for spatial adaptivity.

Keywords: *phase-field, staggered scheme, brittle fracture, hybridizable discontinuous Galerkin (HDG).*
MSC (2010): *35Q74, 74R10, 65M60.*
Received:
Accepted:

Acknowledgement
This work was supported by the AGAUR training grant FI-DGR 2017, the DAFOH2 project (Ministerio de Economía y Competitividad, MTM2013-46313-R) and the Generalitat de Catalunya (2017-SGR-1278).

1. Introduction

Models of fracture in brittle materials can be based on discontinuous and continuous descriptions of cracks.

Discontinuous models describe cracks as sharp entities by means of discontinuous displacement fields. The main disadvantage of these models is the lack of a rigorous strategy to determine initiation and propagation of cracks. Numerically, they are usually tackled by the eXtended Finite Element Method (X-FEM), which enables to solve the problem with meshes unfitted to the crack geometry [2, 16]. However, dealing with discontinuities in a X-FEM setting may be cumbersome in cases with complex patterns [18].

Alternatively, phase-field models for fracture represent cracks as damaged regions that have lost their load-carrying capacity, with continuous displacement fields in all the domain [3]. These models introduce an auxiliar field d, called the *phase-field variable* or *damage field*, which differentiates between the broken and unbroken states of the material and varies smoothly between them. The evolution of the phase-field variable as a result of the loading conditions handles naturally the initiation, propagation, branching and coalescence of cracks. Incorporating the crack evolution into the equations is the main advantage of phase-field models over the discontinuous ones.

The phase-field approach introduces a regularization length parameter ℓ, which comes from the smeared representation of the crack and can be related to its width. Since the goal is to approximate a sharp crack, the parameter ℓ is to be chosen small and the phase-field variable d will vary sharply in the damaged zone. Therefore, high spatial resolution is a key requirement to approximate properly the solution. The usual strategy is to refine the computational mesh locally where the crack is expected to propagate: a priori in the cases in which the crack path is known and by remeshing as the phase-field value evolves when it is not. Obviously, this implies a high computational cost. A reasonable approach to reduce the cost is defining an adaptive refinement method. The different strategies proposed in the literature offer an alternative to remeshing, though they are non-trivial (see [12] and the references therein). We refer to [1, 20] for an exhaustive review of existing phase-field models and the numerical challenges they present.

In this work, we use the Hybridizable Discontinuous Galerkin method (HDG) as an alternative to standard FEM to solve the phase-field equations. HDG was first proposed in [5] for second order elliptic problems and, due to its promising properties, has already been formulated for multiple problems, see for example [10, 13, 17].

As any other Discontinuous Galerkin (DG) method, HDG is based on the use of element-by-element discontinuous basis functions in a finite element setting. Continuity of the solution is imposed in weak form by means of numerical fluxes on element boundaries. DG methods are appealing to solve the equations of the phase-field model because of the possiblity of using different approximation bases in neighbouring elements, which will enable the straightforward definition of an adaptive refinement strategy. Among all DG methods, we choose HDG because it involves less degrees of freedom, with a computational efficiency close to standard continuous FE and better convergence properties [11, 21].

In Section 2 we provide a brief overview of the chosen phase-field model for brittle fracture and the staggered scheme to solve it. In Section 3, we present the HDG formulation of the equations. Finally, in Section 4, we compare the results obtained with the HDG formulation with the ones obtained with standard FEM for a benchmark problem, for both low and high-order degrees of approximation.

2. Phase-field modelling of brittle fracture

In this work, we consider the quasi-static phase-field model for fracture proposed by Bourdin et al. in [3].

Let $\Omega \subset \mathbb{R}^n$, $n = 2, 3$, be an open bounded domain occupied by an elastic body with a traction-free crack denoted by Γ_C and under the hypothesis of small deformations, see Figure 1 (a). Let $\mathbf{u}(\mathbf{x}, t)$ be the displacement field at a point $\mathbf{x} \in \Omega$ at time t and define ε as the standard infinitesimal strain tensor $\varepsilon(\mathbf{u}) = \left(\boldsymbol{\nabla}\mathbf{u} + (\boldsymbol{\nabla}\mathbf{u})^T\right)/2$. The displacement field satisfies Dirichlet and Neumann boundary conditions on Γ_D and Γ_N, respectively, with $\Gamma_D \cup \Gamma_N = \partial\Omega$ and $\Gamma_D \cap \Gamma_N = \emptyset$.

In [6] Francfort and Marigo state that the fracture process acts to minimize the total energy of the body, which can be expressed as the sum of its bulk elastic energy and the crack surface energy, that is

$$E(\mathbf{u}, \Gamma_C) = \int_\Omega \Psi_0(\varepsilon)\, \mathrm{d}V + G_c \int_{\Gamma_C} \mathrm{d}s, \tag{1}$$

with Ψ_0 the elastic energy density and G_C the critical energy release rate. We restrict ourselves to the case of linear elastic isotropic materials, for which the elastic energy density is given by $\Psi_0(\varepsilon) = (\varepsilon : \mathbf{C} : \varepsilon)/2$, with $\mathbf{C}$ the fourth-order elasticity tensor depending on the Lamé parameters.

To enable a numerical treatment of (1), Bourdin et al. [3] introduced a regularized formulation by considering a smeared representation of the sharp crack Γ_C, see Figure 1 (b). The crack is defined by a new field $d(\mathbf{x}, t)$ which varies smoothly between two values representing the unbroken and broken states of the material, 0 and 1 respectively, and is therefore called the *phase-field* or *damage parameter*. The energy functional (1) is then approximated by

$$E_\ell(\mathbf{u}, d) = \int_\Omega \left((1-d)^2 + \eta\right) \Psi_0(\varepsilon)\, \mathrm{d}V + G_c \int_\Omega \left(\frac{d^2}{2\ell} + \frac{\ell}{2}|\nabla d|^2\right) \mathrm{d}V, \tag{2}$$

where ℓ regulates the width of the diffuse crack and η is a small dimensionless parameter to avoid a complete loss of stiffness in broken regions. It has been proved [4] that with $\ell \to 0$, the regularized functional (2) Γ-converges to (1). This implies that the set $\{d = 1\}$ tends to the sharp crack Γ_C as the width of the smeared representation tends to 0.

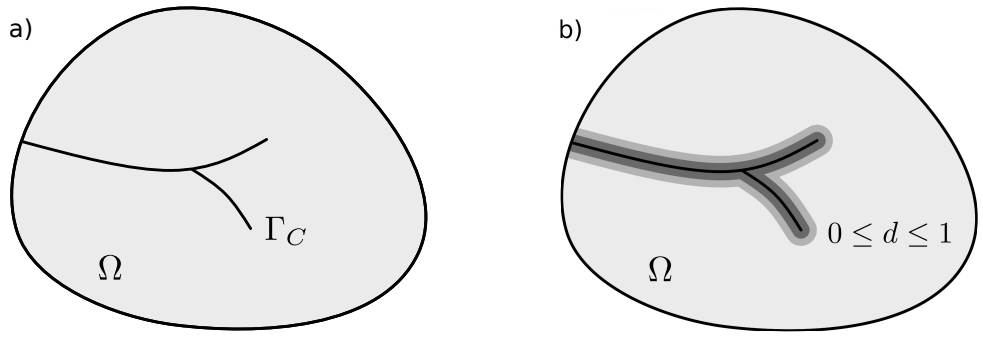

Figure 1: a) Body with a sharp crack Γ_C. b) Smeared crack representation.

Minimizing the energy functional (2) we obtain the system

$$\begin{cases} \nabla \cdot \boldsymbol{\sigma} = \mathbf{0}, \\ -\ell^2 \Delta d + d = \dfrac{2\ell}{G_c}(1-d)\Psi_0, \end{cases} \tag{3}$$

with the stress tensor $\boldsymbol{\sigma}$ defined as

$$\boldsymbol{\sigma}(\mathbf{u}, d) = \left((1-d)^2 + \eta\right) \frac{\partial \Psi_0(\boldsymbol{\varepsilon})}{\partial \boldsymbol{\varepsilon}} = \left((1-d)^2 + \eta\right) \mathbf{C} : \boldsymbol{\varepsilon}(\mathbf{u}). \tag{4}$$

Notice that in the second equation in (3), the energy density $\Psi_0(\mathbf{x}, t)$ acts as a source term for the damage field d. Following Miehe et al. in [14, 15], we replace Ψ_0 in this equation by a history field variable $\mathcal{H}$ defined as

$$\mathcal{H}(\mathbf{x}, t) = \max_{\tau \in [0,t]} \Psi_0(\boldsymbol{\varepsilon}(\mathbf{x}, \tau)),$$

to enforce irreversibility of the crack evolution.

The resulting system of governing equations is to be solved using an incremental procedure for the loading process. The time interval of interest is discretized and, assuming the solution at time $t^{(n)}$ is known, the system is solved at time $t^{(n+1)}$ using the corresponding boundary conditions

$$\begin{cases} \boldsymbol{\sigma} \cdot \mathbf{n} = \mathbf{t}^{(n+1)} & \text{on } \Gamma_N, \\ \mathbf{u} = \mathbf{u}_D^{(n+1)} & \text{on } \Gamma_D, \\ \nabla d \cdot \mathbf{n} = 0 & \text{on } \partial\Omega, \end{cases} \tag{5}$$

where $\mathbf{t}^{(n+1)}$ and $\mathbf{u}_D^{(n+1)}$ are the prescribed tractions and displacements, respectively, and $\mathbf{n}$ stands for the outward unit normal vector.

2.1 Staggered approach

The total energy (2) is convex with respect to $\mathbf{u}$ and d separately, but not with respect to both of them. This motivates the solution of the system by means of a staggered scheme: at each load step, we compute the displacement field $\mathbf{u}$ and the damage field d alternately until convergence. Given the solution $(\mathbf{u}^n, d^n)$ at time t^n, the solution at time t^{n+1} is computed by iterating over i in the following scheme:

1. Compute $\left[\mathbf{u}^{n+1}\right]^{i+1}$ by solving the equation

$$\nabla \cdot \boldsymbol{\sigma}\left(\left[\mathbf{u}^{n+1}\right]^{i+1}, \left[d^{n+1}\right]^{i}\right) = 0 \text{ in } \Omega, \tag{6}$$

   with $\boldsymbol{\sigma}$ given by (4) and boundary conditions $\boldsymbol{\sigma} \cdot \mathbf{n} = \mathbf{t}^{n+1}$ on Γ_N, $\left[\mathbf{u}^{n+1}\right]^{i+1} = \mathbf{u}_D^{n+1}$ on Γ_D.

2. Update the history field $\left[\mathcal{H}^{n+1}\right]^{i+1} = \max\left(\mathcal{H}^n, \left[\Psi_0^{n+1}\right]^{i+1}\right)$.

3. Compute $\left[d^{n+1}\right]^{i+1}$ by solving

$$-\ell^2 \Delta \left[d^{n+1}\right]^{i+1} + \left[d^{n+1}\right]^{i+1} = \frac{2\ell}{G_c}\left(1 - \left[d^{n+1}\right]^{i+1}\right)\left[\mathcal{H}^{n+1}\right]^{i+1} \text{ in } \Omega, \tag{7}$$

   with boundary condition $\left(\nabla \left[d^{n+1}\right]^{i+1}\right) \cdot \mathbf{n} = 0$ on $\partial\Omega$.

We take $(\mathbf{u}^0, d^0)(\mathbf{x}) = (\mathbf{0}, 0)$ for all $\mathbf{x}$ in Ω and $\left[d^{n+1}\right]^0 = d^n$ for $n > 0$. We keep iterating over i until some stopping criterion indicating convergence is satisfied. An alternative is to take sufficiently small load

increments and use the staggered approach without iterating, see for example [1, 8], but the speed of propagation of the crack might be underestimated. Here, we iterate until the relative Euclidean norm of the difference of two consecutive iterates is smaller than a fixed tolerance, for both the displacement and damage fields.

Remark 2.1 (Efficiency). The staggered algorithm is simple and has been proved to be robust [15], but many iterations are needed to reach convergence even for simple benchmark problems. A monolithic scheme computing simultaneously both fields would be more efficient, but then one has to deal with the non-convexity of the functional (2) and the Jacobian matrix of the system being indefinite [9, 19].

3. HDG formulation

We aim to use HDG to solve the governing equations of the phase-field model. The adopted staggered approach enables an independent numerical treatment for each of the equations, so we can focus on the HDG formulations for the linear elasticity equilibrium equation (6) and the damage field equation (7). For the former equation, there are various options in the literature. Here, we consider the HDG formulation for linear elasticity by Soon et al. in [17, 7]. For the latter, we add the reaction term to the standard HDG formulation for diffusion by Cockburn et al. in [5]. Both formulations are recalled in this section.

Throughout the section, we assume the domain Ω covered by a finite element mesh with n_{el} disjoint elements K_i satisfying

$$\bar{\Omega} \subset \bigcup_{i=1}^{n_{el}} \bar{K}_i, \quad K_i \cap K_j = \emptyset \text{ for } i \neq j,$$

and denote the union of the n_{fc} faces Γ_f of the mesh as

$$\Gamma = \bigcup_{i=1}^{n_{el}} \partial K_i = \bigcup_{f=1}^{n_{fc}} \Gamma_f.$$

3.1 HDG for the equilibrium equation

Let us consider the linear elasticity problem defined in (6), to be solved for a frozen damaged field d. The problem can be written in the broken space of elements as a set of local element-by-element equations and some global equations. Local problems impose the linear elasticity equation at each element K_i with Dirichlet boundary conditions, namely

$$\begin{cases} \nabla \cdot \boldsymbol{\sigma}(\mathbf{J}, d) = \mathbf{0} & \text{in } K_i, \\ \mathbf{J} - \boldsymbol{\nabla}\mathbf{u} = \mathbf{0} & \text{in } K_i, \\ \mathbf{u} = \hat{\mathbf{u}} & \text{on } \partial K_i, \end{cases} \tag{8}$$

for $i = 1...n_{el}$. The variable $\mathbf{J}$ is introduced to split the problem into a system of first order PDE and $\hat{\mathbf{u}}$ is a new trace variable defined on the skeleton of the mesh, Γ, which is single-valued, see Figure 2. Note that, given $\hat{\mathbf{u}}$, the local problems (8) can be solved to determine $\mathbf{u}$ and $\mathbf{J}$ at each element.

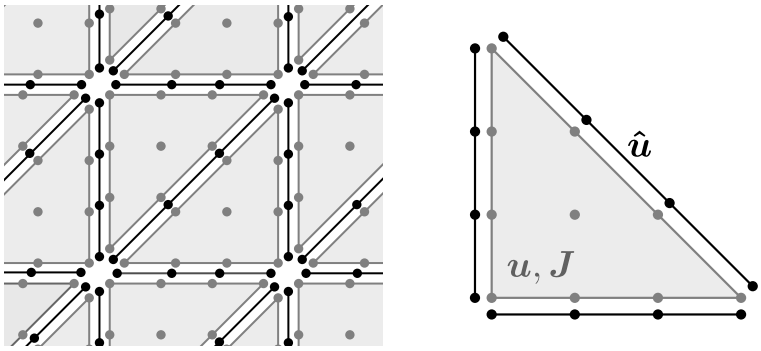

Figure 2: Left: HDG discretization of the domain with the mesh skeleton Γ. Right: detail of the HDG discretization for the local problem in one element.

The global problem is stated to determine the trace variable $\hat{\mathbf{u}}$. It imposes equilibrium of tractions on faces and also the boundary conditions, that is,

$$\begin{cases} [\![\boldsymbol{\sigma} \cdot \mathbf{n}]\!] = \mathbf{0} & \text{in } \Gamma \setminus \partial\Omega, \\ \boldsymbol{\sigma} \cdot \mathbf{n} = \mathbf{t}_N & \text{on } \Gamma_N, \\ \hat{\mathbf{u}} = \mathbf{u}_D & \text{on } \Gamma_D, \end{cases} \tag{9}$$

where $[\![\cdot]\!]$ denotes the jump operator defined at a face Γ_f as $[\![\odot]\!] = \odot_{L_f} + \odot_{R_f}$, where L_f and R_f denote the left and right elements sharing the face and $\odot_i$ denotes the value of $\odot$ from element K_i. Note that the continuity of $\mathbf{u}$ across Γ is satisfied due to the boundary condition $\mathbf{u} = \hat{\mathbf{u}}$ in the local problems and the fact that $\hat{\mathbf{u}}$ is single-valued.

The HDG formulation of the problem is obtained by the discretization of the local and global equations. To approximate the elemental variables, $\mathbf{u}$ and $\mathbf{J}$, and the trace variable, $\hat{\mathbf{u}}$, the discrete spaces considered are

$$\mathcal{V}^h(\Omega) = \{v \in L^2(\Omega) : v|_{K_i} \in \mathcal{P}_p(K_i) \text{ for } i = 1...\mathrm{n_{el}}\},$$
$$\Lambda^h(\Gamma) = \{\hat{v} \in L^2(\Gamma) : \hat{v}|_{\Gamma_f} \in \mathcal{P}_p(\Gamma_f) \text{ for } f = 1...\mathrm{n_{fc}}\},$$

where $\mathcal{P}_p$ denotes the space of polynomials of degree less or equal to p. To simplify the notation, we use $\mathbf{u}$, $\mathbf{J}$, $\hat{\mathbf{u}}$ to denote both the solutions and their approximations.

For an element K_i, the weak form for the local problem (8) is: given $\hat{\mathbf{u}} \in [\Lambda^h(\Gamma)]^n$, find $\mathbf{u} \in [\mathcal{V}^h(K_i)]^n$, $\mathbf{J} \in [\mathcal{V}^h(K_i)]^{n\times n}$ such that

$$\begin{aligned} &\int_{K_i} \mathbf{v} \cdot (\boldsymbol{\nabla} \cdot \boldsymbol{\sigma}) \; \mathrm{d}V + \int_{\partial K_i} \mathbf{v} \cdot ((\mathbf{C} : \tau\,(\hat{\mathbf{u}} - \mathbf{u}) \otimes \mathbf{n}) \cdot \mathbf{n}) \; \mathrm{d}s + \int_{K_i} \mathbf{v} \cdot \mathbf{f} \; \mathrm{d}V = 0, \\ &\int_{K_i} \mathbf{Q} : \mathbf{J} \; \mathrm{d}V + \int_{K_i} (\boldsymbol{\nabla} \cdot \mathbf{Q}) \cdot \mathbf{u} \; \mathrm{d}V - \int_{\partial K_i} (\mathbf{Q} \cdot \mathbf{n}) \cdot \hat{\mathbf{u}} \; \mathrm{d}s = 0, \end{aligned} \tag{10}$$

for all $\mathbf{v} \in [\mathcal{V}^h(K_i)]^n$, for all $\mathbf{Q} \in [\mathcal{V}^h(K_i)]^{n\times n}$. The first equation in (10) is obtained from the first equation in (8) by applying integration by parts, replacing the numerical flux $\hat{\mathbf{J}} := \mathbf{J} + \tau(\hat{\mathbf{u}} - \mathbf{u}) \otimes \mathbf{n}$ on the boundary and undoing the integration by parts. τ is a nonnegative stabilization parameter, which here is taken as a positive constant on all faces.

The discretization of the local problem (10) leads to the so-called *local solver* for each element K_i, which expresses $\mathbf{u}$ and $\mathbf{J}$ in terms of $\hat{\mathbf{u}}$, namely

$$\mathbf{u}_e = \mathbf{U}^{K_i} \boldsymbol{\Lambda}^i + \mathbf{f}_U^{K_i}, \;\; \mathbf{J}_e = \mathbf{Q}^{K_i} \boldsymbol{\Lambda}^i + \mathbf{f}_Q^{K_i}, \tag{11}$$

with matrices $\mathbf{U}^{K_i}, \mathbf{Q}^{K_i}$ and vectors $\mathbf{f}_U^{K_i}, \mathbf{f}_Q^{K_i}$. $\mathbf{\Lambda}^i$ is a vector containing the unknown nodal values of $\hat{\mathbf{u}}$ for all the faces of K_i, this is, $\mathbf{\Lambda}^i := \left[\hat{\mathbf{u}}^{F_{i,1},T}, ..., \hat{\mathbf{u}}^{F_{i,m},T}\right]^T$.

For the global problem (9), the weak form is stated replacing the numerical flux $\hat{\mathbf{J}}$ in $\boldsymbol{\sigma}(\mathbf{J})$. Defining $\hat{\boldsymbol{\sigma}} := \boldsymbol{\sigma}(\hat{\mathbf{J}}) = \boldsymbol{\sigma}(\mathbf{J}) + \mathbf{C} : (\tau(\hat{\mathbf{u}} - \mathbf{u}) \otimes \mathbf{n})$, the weak form is: find $\hat{\mathbf{u}} \in [\Lambda^h(\Gamma)]^n$ such that $\hat{\mathbf{u}} = \mathbf{u}_D$ on Γ_D and

$$\int_\Gamma \hat{\mathbf{v}} \cdot [\![\hat{\boldsymbol{\sigma}} \cdot \mathbf{n}]\!] \, \mathrm{d}s + \int_{\Gamma_N} \hat{\mathbf{v}} \cdot (\hat{\boldsymbol{\sigma}} \cdot \mathbf{n}) \, \mathrm{d}s = \int_{\Gamma_N} \hat{\mathbf{v}} \cdot \mathbf{t}_N \, \mathrm{d}s, \tag{12}$$

for all $\hat{\mathbf{v}} \in [\Lambda^h(\Gamma)]^n$ such that $\hat{\mathbf{v}} = \mathbf{0}$ on Γ_D. Discretizing the global weak form and replacing $\mathbf{u}$ and $\mathbf{J}$ in terms of $\hat{\mathbf{u}}$ by the local solver (11), we get a system for $\hat{\mathbf{u}}$. Once $\hat{\mathbf{u}}$ is determined, using the local solvers (11), we compute $\mathbf{u}$ and $\mathbf{J}$ in every element.

For this formulation, $\mathbf{u}$ converges with order $p+1$ in L^2 norm and $\mathbf{J}$ with order $p+1/2$ [7].

3.2 HDG for the damage field equation

The HDG formulation for the damage field equation (7) is obtained analogously to the formulation for linear elasticity. Introducing a new variable $\mathbf{q}$ to be the gradient of d, the local problems impose the equation in every element K_i with Dirichlet boundary conditions, and their weak form reads: given $\hat{d} \in \Lambda^h(\Gamma)$, find $d \in \mathcal{V}^h(K_i)$, $\mathbf{q} \in [\mathcal{V}^h(K_i)]^n$ such that

$$\begin{aligned}
&-\int_{K_i} G_C \ell \; v \cdot \boldsymbol{\nabla} \cdot \mathbf{q} \, \mathrm{d}V - \int_{\partial K_i} G_C \ell \tau \, (\hat{d} - d) v \, \mathrm{d}s + \int_{K_i} \left(\frac{G_C}{\ell} + 2\mathcal{H} \right) v d \, \mathrm{d}V = \int_{K_i} v 2\mathcal{H}, \\
&\int_{K_i} \mathbf{w} \cdot \mathbf{q} \, \mathrm{d}V + \int_{K_i} (\boldsymbol{\nabla} \cdot \mathbf{w}) d \, \mathrm{d}V - \int_{\partial K_i} \mathbf{w} \cdot \mathbf{n} \, \hat{d} \, \mathrm{d}s = 0,
\end{aligned}$$

for all $v \in \mathcal{V}^h(K_i)$, for all $\mathbf{w} \in [\mathcal{V}^h(K_i)]^n$. The numerical flux prescribed on the boundary of every element is $\hat{\mathbf{q}} := \mathbf{q} + \tau(\hat{d} - d)\mathbf{n}$, with τ the stabilization parameter.

The weak form of the global problem is: find $\hat{d} \in \Lambda^h(\Gamma)$ such that

$$\int_{\Gamma \setminus \partial\Omega} \hat{v} \cdot [\![\hat{\mathbf{q}} \cdot \mathbf{n}]\!] \, \mathrm{d}s = 0,$$

for all $\hat{v} \in \Lambda^h(\Gamma)$.

In this case, both d and $\mathbf{q}$ are proved to converge with order $p+1$ in L^2 norm.

Remark 3.1 ($\mathcal{H}$ is evaluated at integration points). To solve the damage field equation we need the value of $\mathcal{H}$ at integration points. From the staggered scheme, $\mathcal{H}$ can be computed using the nodal values of $\mathbf{J}$ obtained by solving the equilibrium equation. Evaluating $\mathcal{H}$ at nodes may result in negative values when it is interpolated to integration points if we use approximation functions of degree greater than 1, even though it is a nonnegative function by definition. This leads to unphysical solutions. Also, it may cause the non-convergence of the staggered scheme if consecutive iterates alternate negative and positive values at some points. We will illustrate this behavior with a numerical example in next section. To avoid non-physical negative values $\mathbf{J}$ is interpolated to integration points and then these values are directly used to evaluate $\mathcal{H}$.

4. Numerical example: L-shaped panel test

One of the typical benchmark problems in computational fracture is the L-shaped panel test. Consider the specimen in Figure 3 (left), which is fixed on the bottom and has imposed vertical displacement at a 30 mm distance to the right edge. Following [1], the material parameters are $\lambda = 6.16$ kN/mm^2, $\mu = 10.95$ kN/mm^2 and $G_c = 8.9 \cdot 10^{-5}$ kN/mm^2. The regularization length in the phase-field model is taken to be $\ell = 3$ mm and the residual stiffness is $\eta = 10^{-5}$. The stabilization parameter appearing in the HDG formulation of the equations is taken $\tau = 1$ for both the equilibrium and the damage field equations.

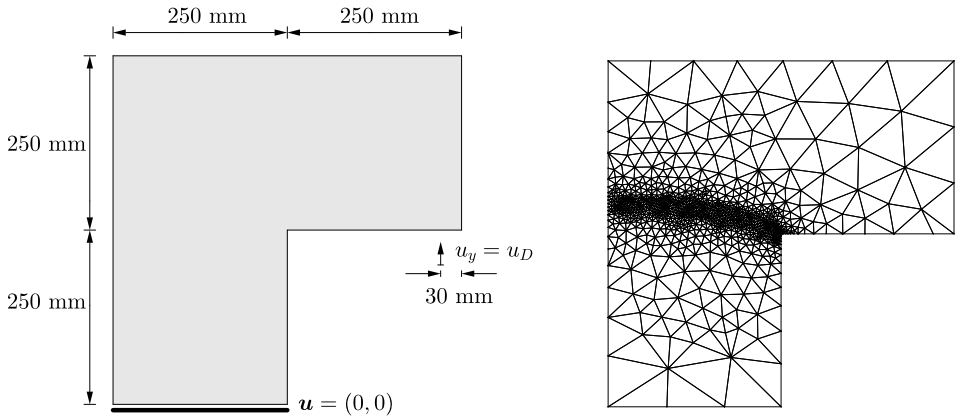

Figure 3: Left: geometry and boundary conditions of the test. Right: computational mesh.

We consider a triangular mesh with 1842 elements, pre-refined along the expected crack path with a mesh size of $h_{ref} = 3.5$ mm, see Figure 3 (right), and four nested meshes to this one obtained by dividing the mesh size by two for each level of refinement. The problem is solved with increments in the prescribed vertical displacement of $\Delta u_D = 10^{-3}$ mm and we iterate in the staggered scheme for each load step until convergence is reached with a tolerance of 10^{-6}.

Remark 4.1 (Boundary conditions). Imposing the vertical displacement at just one point causes unphysical damage near the point. To cancel this out and impose properly the boundary conditions, we set the damage to zero in the region after every iteration of the staggered scheme. Another strategy would be to assign a higher value of G_C where needed [20].

Comparison of FEM and HDG. We start by considering linear approximation functions. As expected, the solution tends to converge when refining the mesh, as it can be observed in the load-displacement curves in Figure 4. We obtain similar results for both FEM and HDG, with slightly better accuracy in HDG. Recall that HDG has a better order of convergence for the gradient of the displacement field $\mathbf{J}$.

Spatial resolution. Using degree of approximation $p = 1$, the primary mesh with $h_{ref} = 3.5$ mm is not fine enough to approximate properly the smeared crack with $\ell = 3$ mm. The smeared crack becomes mesh-dependent and has a width of one element, see Figure 5. In Figure 6, we plot the damage field for different imposed displacements of the loading process with the 2-nested level mesh. The crack path obtained in this case is comparable with the results in the literature [1, 8].

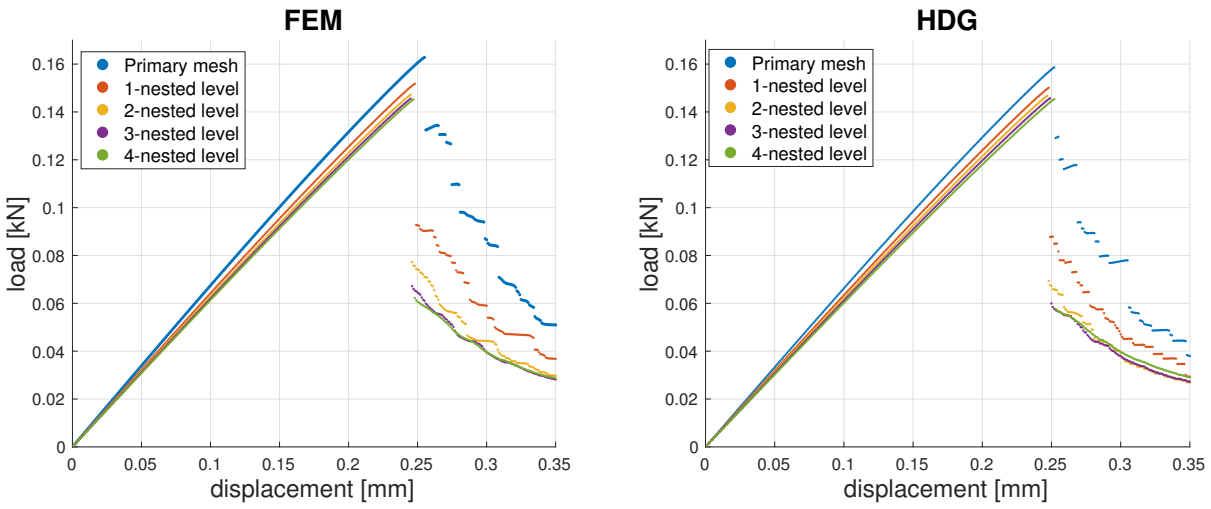

Figure 4: Load-displacement curves for the L-shaped panel test when using $p = 1$ for both FEM and HDG.

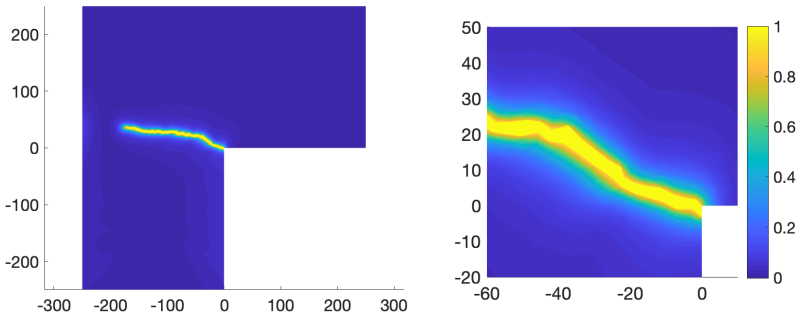

Figure 5: Damage field obtained with HDG at an imposed displacement of $u_D = 0.45$ mm. Degree of approximation $p = 1$, primary mesh and $\ell = 3$ mm.

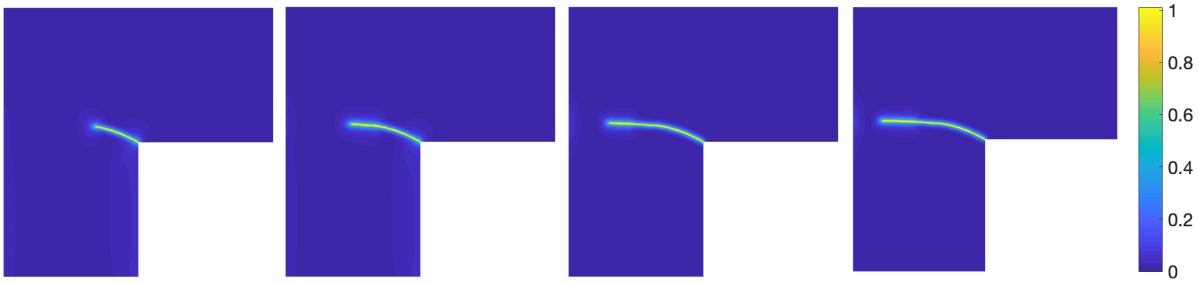

Figure 6: Damage field at displacements (a) $u_D = 0.25$ mm, (b) $u_D = 0.3$ mm, (c) $u_D = 0.4$ mm, (d) $u_D = 0.5$ mm. Degree of approximation $p = 1$, 2-nested level mesh and $\ell = 3$ mm.

Computation with high-order approximations. To increase the accuracy in space needed to capture the profile of the solution, one can take higher degree p of the approximation basis functions. With $p = 5$, we expect to obtain more accurate results than with $p = 1$ for the same mesh. Indeed, in Figure 7 (left), we compare the load-displacement curve obtained with degree $p = 1$ and the 4-nested level mesh with the curves obtained for $p = 5$ and coarser meshes. In this case, using a higher-order degree of approximation gives us the same order of accuracy in the solution and with less degrees of freedom. In Figure 7 (right),

we note that solving for $p = 5$ with the primary mesh we no longer observe the mesh dependence we have for $p = 1$ due to low spatial resolution.

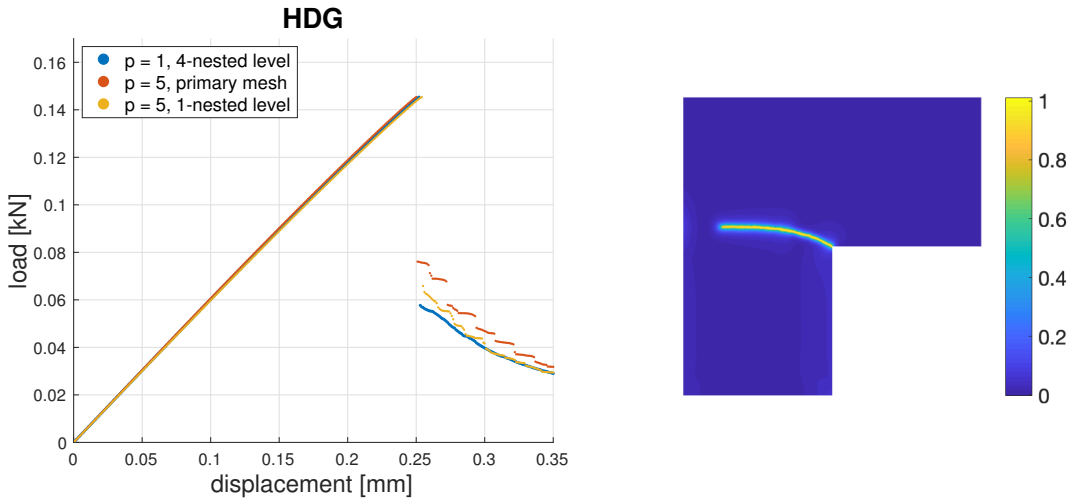

Figure 7: Left: load-displacement curves obtained with $p = 5$. Right: damage field at $u_D = 0.45$ mm for $p = 5$ and the primary mesh.

Importance of evaluating $\mathcal{H}$ at integration points. As commented in remark 3.1, if $\mathcal{H}$ is evaluated at nodes and then interpolated to Gauss points, it can reach negative values when using shape functions of degree $p > 1$. To illustrate this phenomenon, consider the L-shaped panel test with the primary mesh and degree of approximation $p = 5$. If we evaluate $\mathcal{H}$ at nodes, the damage field d is no longer in the interval $[0, 1]$. In Figure 8, we can see the damage field obtained with this formulation for imposed vertical displacement $u_D = 0.247$ mm. Both the values of d and the pattern obtained are not a proper solution of the problem: the damage field presents oscillations and gets a value of 1.2 at the corner.

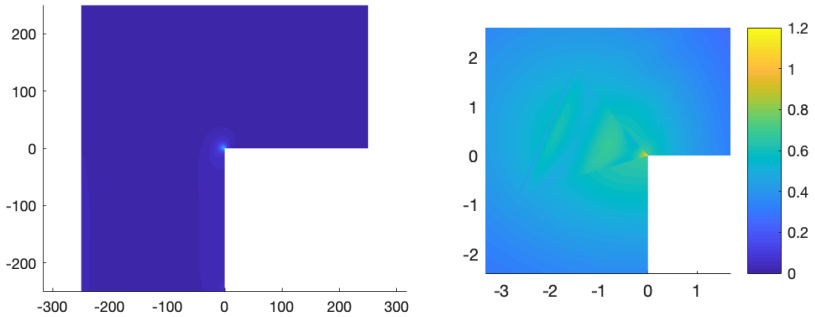

Figure 8: Evaluating $\mathcal{H}$ at nodes. Damage field for $u_D = 0.247$ mm. Whole body on the left, zoom on the right. Degree of approximation $p = 5$, primary mesh. The solution obtained is unphysical.

For the next load step, corresponding to imposed displacement $u_D = 0.248$ mm, the staggered scheme does not converge. In Figure 9, we plot the relative Euclidean norm of the difference of consecutive iterates for d and the maximum and minimum values of damage obtained. Notice that the absolute value of the damage field gets arbitrarely large.

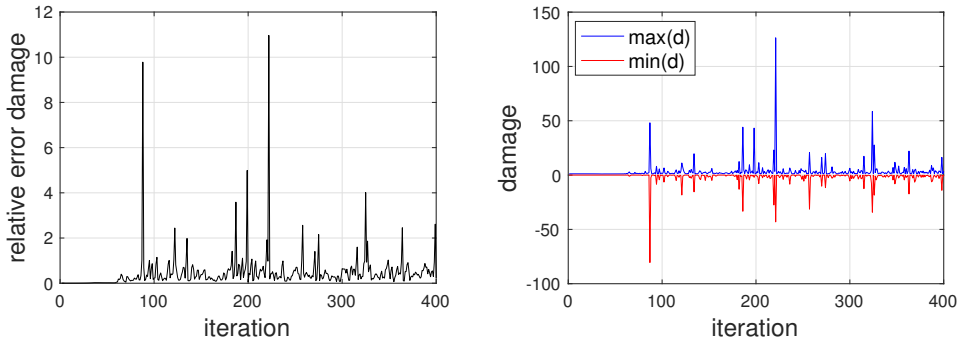

Figure 9: Evaluating $\mathcal{H}$ at nodes. For imposed displacement $u_D = 0.248$ mm, relative error of d (left) and maximum/minimum values of d (right) for number of iteration. The staggered scheme does not converge in this case.

5. Conclusions

We have proposed an HDG approach for phase-field models of brittle fracture using a staggered scheme that enables to uncouple the system. We have compared this formulation with the classical FEM formulation in a numerical example and both of them present the same behavior. As expected, the solution is more accurate when refining the mesh or increasing the degree of approximation. With HDG we obtain better accuracy than with FEM for the same mesh and degree of approximation, but at the price of a higher computational cost.

The main drawback of phase-field models is their inefficiency coming from the remeshing needed if the crack path is not known. The HDG formulation is interesting for this problem because of the suitability of the method for adaptivity. The implementation of p-adaptivity and h-adaptivity for this formulation is subject of ongoing work.

References

[1] M. Ambati, T. Gerasimov, L. De Lorenzis. *A review on phase-field models of brittle fracture and a new fast hybrid formulation*, Comput Mech (2015) 55:383–405.

[2] T. Belytschko, T. Black. *Elastic crack grow in finite element with minimal remeshing*, Int J Numer Methods Eng (1999) 45(5):601–620.

[3] B. Bourdin, G.A. Francfort, J.J. Marigo. *Numerical experiments in revisited brittle fracture*, J Mech Phys Solids (2000) 48:797–826.

[4] B. Bourdin, G.A. Francfort, J.J. Marigo. *The variational approach to fracture*, Journal of Elasticity (2008) 91(1-3):5–148.

[5] B. Cockburn, J. Gopalakrishnan, R. Lazarov. *Unified hybridization of discontinuous Galerkin, mixed and continuous Galerkin methods for second order elliptic problems*, SIAM J Numer Anal (2009) 47:1319–1365.

[6] G.A. Francfort, J.J. Marigo. *Revisiting brittle fracture as an energy minimization problem*, Journal of Mechanics and Physics of Solids (1998) 46(8):1319–1342.

[7] G. Fu, B. Cockburn, H. Stolarski. *Analysis of an HDG method for linear elasticity*, Int J Numer Methods Eng (2015) 102:51–575.

[8] R. Geelen, Y. Liu, J.E. Dolbow, A. Rodríguez-Ferran. *An optimization-based phase-field method for continuous-discontinuous crack propagation*, Int J Numer Methods Eng (2018) 116:1–20.

[9] T. Gerasimov, L. De Lorenzis. *A line search monolithic approach for phase-field computing of brittle fracture*, Comput Methods Appl Mech Engrg (2016) 312:276–303.

[10] G. Giorgiani, D. Modesto.,S. Fernández-Méndez, A. Huerta. *High-order continuous and discontinuous Galerkin methods for wave problems*, Int J Numer Methods Fluids (2013) 73(10):883–903.

[11] R.M. Kirby, S.J. Sherwin, B. Cockburn. *To CG or to HDG: A Comparative Study*, J Sci Comput (2012) 51:183–212.

[12] S. Nagaraja, M. Elhaddad, M. Ambati, S. Kollmannsberger, L. De Lorenzis, E. Rank. *Phase-field modeling of brittle fracture with multi-level hp-FEM and the finite cell method*, Comput Mech (2018).

[13] N.C. Nguyen, J. Peraire. *Hybridizable discontinuous Galerkin methods for partial differential equations in continuum mechanics*, Journal of Computational Physics (2012) 231:5955–5988.

[14] C. Miehe, F. Welschinger, M. Hofacker. *Thermodynamically consistent phase-field models of fracture: variational principles and multi-field FE implementations*, Int J Numer Methods Eng (2010) 83:1273–1311.

[15] C. Miehe, M. Hofacker, F. Welschinger. *A phase-field model for rate-independent crack propagation: robust algorithmic implementation based on operator splits*, Comput Methods Appl Mech Eng (2010) 199:2765–2778.

[16] N. Moës, J. Dolbow, T. Belytschko. *A finite element method for crack grow without remeshing*, Int J Numer Methods Eng (1999) 46:131–150.

[17] S.C. Soon, B. Cockburn, H.K. Stolarski. *A hybridizable discontinuous Galerkin method for linear elasticity*, Int J Numer Methods Eng (2009) 80:1058–1092.

[18] N. Sukumar, J. Dolbow, N. Moës. *Extended finite element method in computational fracture mechanics: a retrospective examination*, Int J Fract (2015) 196:189–206.

[19] T. Wick. *Modified Newton methods for solving fully monolithic phase-field quasi-static brittle fracture propagation*, Comput Methods Appl Mech Engrg (2017) 325:577–611.

[20] J.Y. Wu, V.P. Nguyen, C.T. Nguyen, D. Sutulas, S. Bordas, S. Sinaie. *Phase field modelling for fracture*, Advances in Applied Mathematics (2018) 53.

[21] S. Yakovlev, D. Moxey, R.M. Kirby, S.J. Sherwin. *To CG or to HDG: A comparative study in 3D*, J Sci Comput (2015) 67(1):192–220.